JBC ARTICLE

Myristoylated methionine sulfoxide reductase A is a late endosomal protein

Received for publication, October 16, 2017, and in revised form, March 19, 2018 Published, Papers in Press, March 28, 2018, DOI 10.1074/jbc.RA117.000473

Jung Mi Lim, Jung Chae Lim, Geumsoo Kim, and Rodney L. Levine[1]

From the Laboratory of Biochemistry, NHLBI, National Institutes of Health, Bethesda, Maryland 20892

Edited by Ursula Jakob

Methionine residues in proteins provide antioxidant defense by reacting with oxidizing species, which oxidize methionine to methionine sulfoxide. Reduction of the sulfoxide back to methionine is catalyzed by methionine sulfoxide reductases, essential for protection against oxidative stress. The nonmyristoylated form of methionine sulfoxide reductase A (MSRA) is present in mitochondria, whereas the myristoylated form has been previously reported to be cytosolic. Despite the importance of MSRA in antioxidant defense, its *in vivo* binding partners and substrates have not been identified. Starting with a protein array, and followed by immunoprecipitation experiments, colocalization studies, and subcellular fractionation, we identified the late endosomal protein, StAR-related lipid transfer domain–containing 3 (STARD3), as a binding partner of myristoylated MSRA, but not of nonmyristoylated MSRA. STARD3 is known to have both membrane-binding and cytosolic domains that are important in STARD3-mediated transport of cholesterol from the endoplasmic reticulum to the endosome. We found that the STARD3 cytosolic domain localizes MSRA to the late endosome. We propose that the previous conclusion that myristoylated MSRA is strictly a cytosolic protein is artifactual and likely due to vigorous overexpression of MSRA. We conclude that myristoylated MSRA is a late endosomal protein that may play a role in lipid metabolism or may protect endosomal proteins from oxidative damage.

Until relatively recently, the functions of methionine in proteins have been poorly defined, except of course, for its role in protein initiation. Biochemistry texts often treat it as a generic hydrophobic amino acid, but investigations from many laboratories have changed this view (1–8). Methionine in proteins functions in antioxidant defense, protein structure, and redox sensing and regulation.

Methionine residues provide antioxidant defense through reversible oxidation and reduction. Methionine is rather readily oxidized to methionine sulfoxide (9, 10) by reactive oxygen and nitrogen species. Oxidation of methionine creates a chiral center at the sulfur so that the methionine sulfoxide produced is a mixture of the *S* and *R* epimers (11). Reduction of the sulfoxide back to methionine is catalyzed by the methionine sulfoxide reductases (MSR),[2] enzymes found in almost all organisms from microbes to humans (12). Recycling by the reductases allows the methionine residue to react again with oxidizing species, creating a system with catalytic efficiency in scavenging reactive species.

MSRA acts on the *S* epimer, and MSRB acts on the *R* epimer. The A class was described some years ago and has been characterized in considerable detail, especially by Weissbach, Brot, and colleagues (12). The B class of reductases, some of which are selenoproteins in higher animals, was discovered more recently and has also been studied intensively (13, 14). Mammals have 3 isoforms of the B class, and one of the A class. There is only one gene for MSRA, but it has two initiation sites (15). Initiation at the first site generates a protein with a mitochondrial targeting sequence. The protein produced by initiation at the second site lacks the mitochondrial targeting sequence and is myristoylated. In monkey kidney and HEK293 cells transfected with the full-length gene, the myristoylated form has been localized to the cytoplasm (~75%) and the nonmyristoylated form to mitochondria (~25%) (15, 16). The role of myristoylation is ill-defined, but the myristoylated form protects the heart against ischemia-reperfusion injury, whereas a cytosolic, nonmyristoylated form does not (17). Myristoylation increases the catalytic efficiency of MSRA *in vitro* by improving its interaction with substrates (18, 19), perhaps by stabilizing an encounter complex (20).

The *in vivo* importance of the reductases is well-established, particularly for MSRA. Knocking out the enzyme caused increased susceptibility to oxidative stress in mice (21), yeast (22), and bacteria (23–26). Conversely, overexpressing MSRA conferred increased resistance to oxidative stress in *Drosophila* (27), *Saccharomyces* (28), *Arabidopsis* (29), PC-12 cells (30), and human T cells (28). *Helicobacter pylori*, a causative agent of gastric ulcers and carcinoma, requires MSRA for protection against oxidative stress, and MSRA appears to act through reduction of methionine sulfoxide in the bacterial catalase (26, 31). Despite the importance of the reductase in defense against oxidative stresses, the mechanisms of its action and even its *in vivo* binding partners and substrates are essentially unknown.

Work by several investigators has established the surprising ability of cells to increase the methionine content of their pro-

This work was supported by the National Institutes of Health NHLBI intramural research program (Grant ZIA HL000225). The authors declare that they have no conflicts of interest with the contents of this article. The content is solely the responsibility of the authors and does not necessarily represent the official views of the National Institutes of Health.

[1] To whom correspondence should be addressed: NHLBI, National Institutes of Health, Bldg. 50 Rm. 2351, Bethesda, MD 20892-8012. E-mail: rlevine@nih.gov.

[2] The abbreviations used are: MSR, methionine sulfoxide reductase; PMSF, phenylmethanesulfonyl chloride; STARD3, StAR-related lipid transfer domain-containing 3; ARF1, ADP-ribosylation factor 1.

Table 1
Candidate interacting proteins with Z score ≥2 from the protein array
The Z score indicates how far and in what direction the value of an individual data point in a population falls from the mean in units of standard deviations.

ID	Name	Z score	CV[a]
NM_006804.2	StAR-related lipid transfer (START) domain containing 3 (STARD3)	7.83	0.04
BC014298.1	PRKR interacting protein1 (IL11 inducible) (PRKRIP1)	5.60	0.11
BC022270.1	CDKN2A interacting protein (CDKN2AIP)	2.18	0.06
NM_004060.2	Cyclin G1 (CCNG1), transcript variant 1	2.01	0.05
NM_207035.1	UPF0471 protein C1orf63 homolog	2.00	0.04

[a] CV, coefficient of variation.

teins when exposed to oxidative stress (7, 32). The mechanism was elucidated by Kim and colleagues (8) who showed that ERK1/2 phosphorylates methionyl tRNA synthetase in cells experiencing oxidative stress. The phosphorylation renders the synthetase promiscuous, due to increased affinity for non-methionine tRNAs, thus increasing the methionine content of proteins during oxidative stress.

Cyclic oxidation and reduction of methionine residues, like any reversible covalent modification, has the potential to function as a regulatory switch. This function has been established for the cytosolic MSRB1. The oxidoreductase MICAL mediates the stereospecific oxidation of Met-44 in actin, leading to depolymerization of actin (6). The cytosolic MSRB1 reduces methionine sulfoxide 44 (MetO-44) back to Met, restoring its ability to polymerize (4, 5). MSRA is a bifunctional enzyme, capable of stereospecifically oxidizing Met and reducing methionine sulfoxide residues, although no *in vivo* substrates have yet been identified (33).

Many proteins with methionine sulfoxide residues have been shown to be substrates of MSRA *in vitro*, although thus far no *in vivo* substrates nor binding partners have been confidently identified. We previously attempted to find interacting proteins *in vivo* using a variety of techniques, but none led to confirmed substrates. The methods used included immunoprecipitation, affinity purification, chemical cross-linking, yeast two-hybridization, HPLC-MS (34), and *in vivo* labeling of endogenous proteins with photoactivatable methionine and leucine (35). We now report that late endosomes are the primary subcellular localization site of myristoylated MSRA and that the previously reported cytosolic localization is an artifact of too robust overexpression in transfected cells. Myristoylated MSRA is anchored to the late endosome by interaction with STARD3, an interaction initially detected with a protein array of human proteins. STARD3 is anchored in the membrane of late endosomes and functions to transfer lipids between organelles, notably cholesterol from the endoplasmic reticulum into late endosomes (36–38). The interaction of STARD3 and myristoylated MSRA clarifies the role of myristoylation of MSRA and broadens the possible *in vivo* functions of MSRA.

Results

A protein array identifies STARD3 as a candidate binding partner of MSRA

We utilized a microprotein array to identify candidate binding partners of MSRA. The arrays are printed on nitrocellulose, are the same dimensions as cDNA arrays used for transcriptomics, and are scanned in the same instruments as cDNA arrays. The protein array we used has 9,483 human proteins, produced in baculovirus with glutathione *S*-transferase tags (39). Cys-74[3] is required for catalytic activity, and thus, C74S lacks both reductase and oxidase activities. We utilized it to facilitate capture of substrates that would bind and not be readily released. We incubated the arrays with biotinylated human myristoylated C74S MSRA and interrogated the array with streptavidin tagged with Alexa Fluor 647. Several candidate proteins emerged, although all but one had relatively low confidence scores (Table 1). The one high confidence candidate was STARD3, a late lysosomal protein located in the lysosomal membrane with a cytosolic domain (40).

Myristoylated MSRA binds to STARD3 in vivo

To test whether MSRA actually interacts with STARD3 within the cell, we co-transfected HEK293 cells with FLAG-tagged *Stard3* and WT or C74S myristoylated *MsrA*. A homogenate was then immunoprecipitated with anti-FLAG antibody. Fig. 1*A* shows that MSRA was co-precipitated with STARD3. Interaction occurred with both the active site mutant and the WT MSRA. Although STARD3 can be detected in non-transfected HEK293 cells, MSRA cannot (15). By transfecting the HEK293 cells only with MSRA, we examined whether it would interact with STARD3 present at normal intracellular concentration, and we again found that both the active-site mutant and the WT enzyme interacted with STARD3 (Fig. 1*C* and *D*).

We then tested whether myristoylation affects the interaction of MSRA and STARD3. Gly-24 is the myristoylated residue in MSRA, so that G24A MSRA is not myristoylated. The G24A MSRA did not interact with STARD3 (Fig. 2*A*). STARD3 has a well-defined cholesterol-binding site (40) that might accommodate a myristoyl moiety. This raises the question of whether STARD3 interacts specifically with myristoylated MSRA or generally with myristoylated proteins. We investigated whether ARF1 (ADP-ribosylation factor 1) interacted with STARD3. ARF1 is a GTPase that is important in protein trafficking and in vesicle budding and uncoating within the Golgi (41). We chose ARF1 because it is myristoylated and its myristoylated-binding site shares similarities with that of MSRA (18). Coexpressing ARF1 and STARD3 in HEK293 cells revealed that STARD3 did not interact with either myristoylated nor nonmyristoylated ARF1 (Fig. 2*C*). We conclude that STARD3 does not bind non-specifically to myristoylated proteins. Rather, it interacts specifically with myristoylated MSRA.

[3] Residues are numbered from the genomic sequence. Initiation at Met-1 produces the mitochondrially-targeted MSRA, whereas initiation at Met-23 produces the non-mitochondrial form (15). After removal of Met-23, Gly-24 becomes the amino terminal residue and is myristoylated.

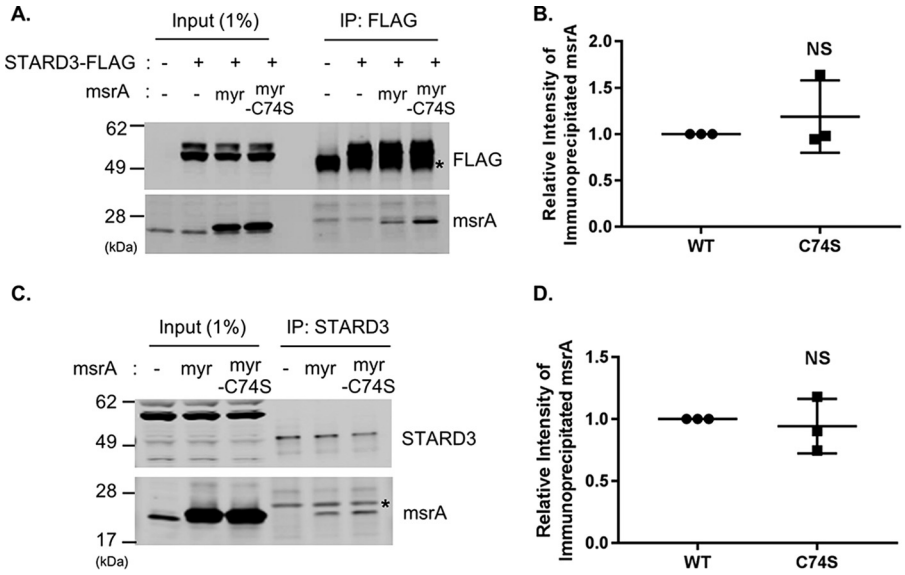

Figure 1. Myristoylated MSRA interacts with STARD3. *A,* HEK293 cells coexpressing FLAG-tagged STARD3 and either the WT or active site mutant (C74S) of myristoylated MSRA were immunoprecipitated with anti-FLAG antibody and probed with anti-MSRA antibody. Both the WT and active site mutant strongly interact with STARD3. The *asterisk* marks the IgG heavy chain. The molecular size markers of protein are indicated in kDa. *B,* quantitation of 3 replicates of the experiment shown in *panel A*, run on separate days. The fluorescence intensity of the WT was set to 1.0. The mean ± S.D. are shown as *lines*. *NS*, not significantly different from the WT with a paired two-tailed *t* test, $p = 0.45$. *C,* myristoylated *MsrA* alone was transfected in HEK293 cells. Endogenous STARD3 was immunoprecipitated with mouse anti-STARD3 antibody and detected by an anti-STARD3 antibody. MSRA was detected by an anti-MSRA antibody. The *asterisk* marks a nonspecific band. *myr*, myristoylated. *D,* quantitation of 3 replicates of the experiment shown in *panel C*, run on separate days. The fluorescence intensity of the WT was set to 1.0. The mean ± S.D. are shown as *lines*. *NS*, not significantly different from the WT with a paired two-tailed *t* test, $p = 0.67$.

Myristoylated MSRA colocalizes with STARD3 at late endosomes

STARD3 is localized to late endosomes (36). An N-terminal domain (MENTAL) has 4 transmembrane helices that embed in the late endosomal membrane (42). MENTAL is followed by the START domain that is cytosolic and contains the lipid-binding domain. We expressed FLAG-tagged STARD3 in COS7 cells and confirmed that it colocalized with the late endosomal marker LAMP1 but not the early endosomal marker EEA1 (Fig. 3, *A* and *B*). Expression of myristoylated MSRA revealed that it colocalized with the late endosomal marker LAMP1 (Fig. 3*C*) and with STARD3 (Fig. 3*D*). The active site mutant also colocalized with STARD3 (Fig. 3*E*). Myristoylated MSRA did not colocalize with the mitochondrial marker DsRed-Mito (Fig. 4). Because of the small size of endosomes, it was difficult to determine whether MSRA was in the interior of the endosome or on its membrane. Treatment of cells with ammonium chloride causes enlargement of endosomes, allowing demonstration that myristoylated MSRA localizes to the late endosomal membrane, whereas nonmyristoylated MSRA does not (Fig. 5).

We then performed subcellular fractionation of liver from WT and MSRA knockout mice, using a sucrose gradient. STARD3 and the late endosomal marker, RAB7, were prominent in the first fraction, as expected for late endosomes (Fig. 6). Myristoylated MSRA was also most prominent in the fraction, confirming the presence of both STARD3 and myristoylated MSRA in nontransgenic mouse liver.

We next investigated the effect of reducing the endogenous level of STARD3 in COS7 cells by treatment with an siRNA against STARD3. Fig. 7 shows that knocking down the level of STARD3 reduced the amount of myristoylated MSRA localized to the late endosome. This provides additional support for the conclusion that MSRA and STARD3 interact directly and not simply through mutual interaction with a third protein.

Fig. 7*D* shows that both myristoylated MSRA and STARD3 levels decrease by about half in response to the siRNA. Fig. 7*E* presents the colocalization of the two proteins. Without siRNA, colocalization is quite high, with a Pearson's correlation coefficient of 0.8. With siRNA, there is a modest, but statistically significant, decrease in colocalization, with a correlation coefficient of 0.6. Although a change in the level of STARD3 might alter the expression of genetically encoded MSRA, one would not expect the synthesis of the transfected GFP-myristoylated MSRA to be affected by a change in STARD3, although it was (Fig. 7). We suggest that the decreased level of the GFP-myristoylated MSRA is due to increased degradation of the fraction not bound to late endosomes.

STARD3 features affecting interaction with myristoylated MSRA

The crystal structure of the cytosolic START domain of STARD3 was solved by Tsujishita and Hurley (40) who showed that cholesterol binds in a hydrophobic tunnel formed by a U-shaped β-barrel and helix α4, which forms a roof over the barrel. They pointed out that Met-307 and Asn-311 are conserved, uncharged residues that influence binding specificity; the double mutant, M307R/N311D, could not bind cholesterol. The N-terminal domain that forms helix α1 does not participate in forming the lipid-binding site but could be the docking site for MSRA. Helix α4 forms a roof over the lipid-binding site and might regulate access to that site. We investigated whether these features affected the interaction of MSRA with STARD3. First, we compared the full-length STARD3 and its cytosolic

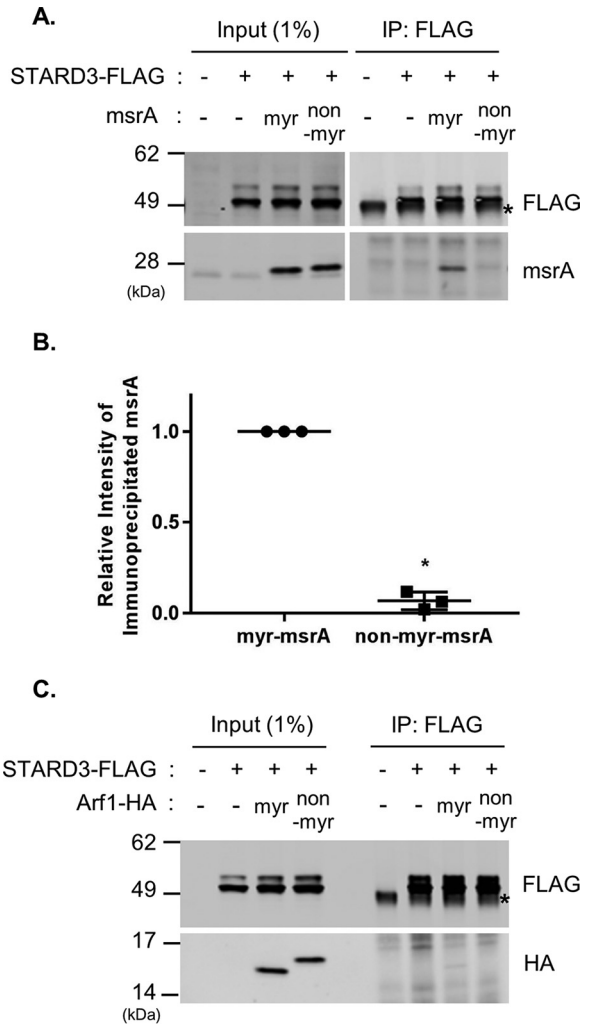

Figure 2. STARD3 interacts only with myristoylated MSRA. *A,* FLAG-tagged STARD3 was coexpressed in HEK293 cells with myristoylated or non-myristoylated MSRA. Cell lysates were immunoprecipitated with anti-FLAG antibody and probed with an anti-MSRA antibody. The *asterisk* marks the IgG heavy chain. *B,* quantitation of 3 replicates of the experiment shown in *panel A*, run on separate days. The fluorescence intensity of the myristoylated MSRA was set to 1.0. The mean ± S.D. are shown as *lines*. *, $p < 0.0001$ with the paired two-tailed *t* test. *C,* myristoylated or nonmyristoylated ARF1, tagged with HA at its C terminus, was overexpressed with FLAG-tagged STARD3 in HEK293 cells. Cell lysates were immunoprecipitated with anti-FLAG antibody and detected by anti-HA antibody. The *asterisk* marks the heavy chain of IgG. This experiment was performed 3 times on separate days, none of which detected an interaction between ARF1 and STARD3.

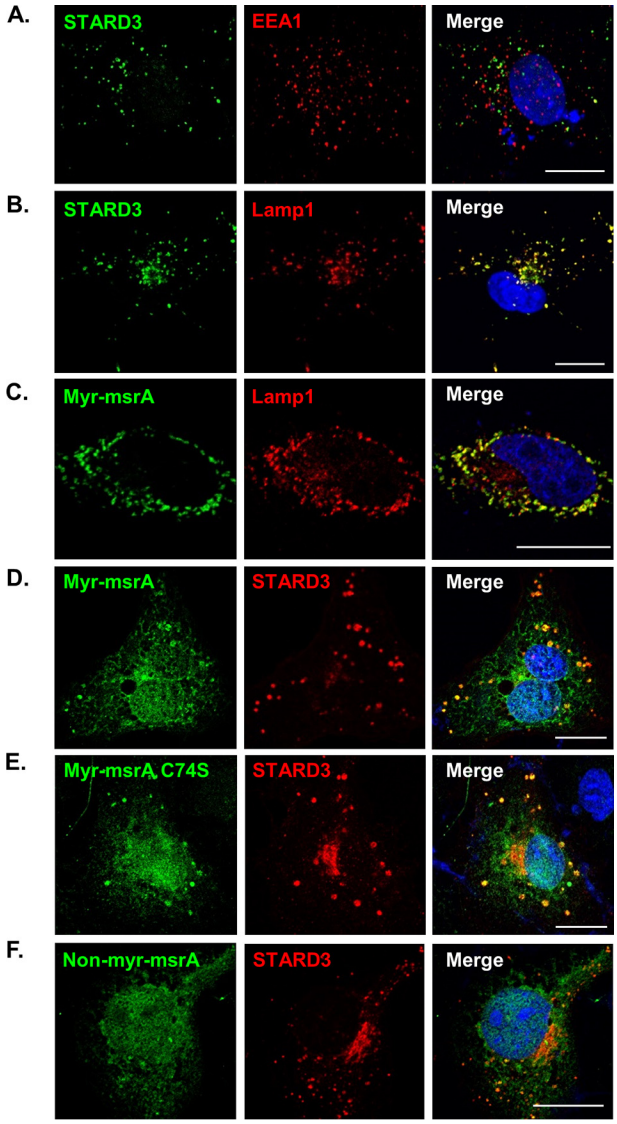

Figure 3. Myristoylated MSRA is colocalized with STARD3 at the late endosome. *A* and *B,* COS7 cells expressing FLAG-tagged STARD3 were stained with anti-EEA1, an early endosome marker (*A*) and anti-LAMP1, a late endosome marker (*B*). *C,* myristoylated *MsrA* was transiently transfected in COS7 cells, which were stained with anti-MSRA and anti-LAMP1. *D–F, MsrA* and FLAG-tagged *Stard3* were transiently transfected in COS7 cells, which were stained with anti-MSRA and anti-FLAG. *D,* the myristoylated form of MSRA was expressed. *E,* the inactive form of myristoylated MSRA (C74S) was expressed. *F,* the nonmyristoylated form of MSRA was expressed. *Scale bars*, 20 μm.

START domain (residues 231–444 of STARD3) that was utilized in the crystal structural studies (40, 44). We found no difference in their interaction with myristoylated MSRA, consistent with the immunohistochemical localization of binding to the cytosolic-facing membrane of late endosomes (Fig. 8*A*). All other studies were then performed with the cytosolic START domain. The mutant that could not bind lipid, M307R/N311D, was also impaired in binding MSRA. Deletion of the N-terminal helix α1 greatly increased binding, whereas deletion of helix α4 modestly increased binding (Fig. 8, *B* and *C*). Thus, neither of those helices is required for MSRA binding. Met-307 is within the binding pocket for lipids, and a recent high-resolution crystal structure shows the sulfur of Met-307 is just 3.8 Å from Trp-310, forming a bond with the aromatic ring (3, 45). We therefore also evaluated the effect of mutating just Met-307 and found that the interaction of STARD3 and MSRA was greatly reduced (Fig. 8, *D* and *E*).

Oxidized STARD3 is a substrate for MSRA

In addition to Met-307, STARD3 has one other methionine residue, Met-427. To determine whether methionine sulfoxide in STARD3 is a substrate for MSRA, we prepared oxidized STARD3 by treating it with hypochlorite to oxidize methionine to methionine sulfoxide. The oxidation conditions yielded proteins with a low fractional oxidation of the methionine residues, as might be expected occur *in vivo*. We then incubated the oxidatively modified protein with MSRA and quantitated the

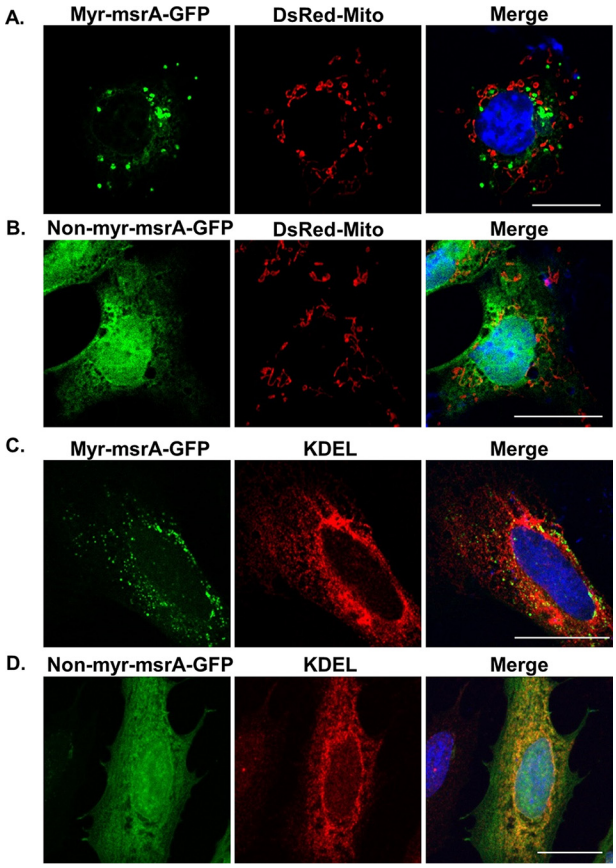

Figure 4. Neither myristoylated MSRA nor nonmyristoylated MSRA is localized to mitochondria or the endoplasmic reticulum. *A* and *B*, COS7 cells were cotransfected with either myristoylated *MsrA-gfp* (*A*) or nonmyristoylated *MsrA* (*B*) and *DsRed-Mito*, a mitochondrial marker protein. *C* and *D*, HeLa cells expressing either myristoylated MSRA-GFP (*C*) or nonmyristoylated MSRA (*D*) were stained with anti-KDEL, an endoplasmic reticulum marker protein. *Scale bars*, 20 μm.

fraction of methionine sulfoxide at positions 307 and 427 that were reduced. methionine sulfoxide 307 was a substrate for MSRA (Fig. 9*A*), whereas the effect on methionine sulfoxide 427 did not reach statistical significance (Fig. 9*B*).

Reconciliation with earlier reports

As noted in the Introduction, Kim and Gladyshev (15, 16) and we previously reported that the nonmitochondrial form of MSRA is cytosolic. That conclusion was based on studies of monkey kidney cells (CV-1 or COS) transfected with the MSRA gene. Neither paper reported the amount of DNA used for transfection, but a review of our laboratory notebooks found that it was 1 μg. Given the results above that demonstrate a late endosomal localization, we wondered whether the amount of DNA used in the earlier studies may have been excessive, saturating the binding sites on late endosomes and leading to accumulation of the excess MSRA in the cytosol. We examined that possibility by transfecting COS7 cells with varying amounts of DNA (Fig. 10). With 0.125 or 0.25 μg of DNA, MSRA colocalized to late endosomes. Although that colocalization was maintained with 0.50 and 0.75 μg of DNA, the cytosol was now flooded with MSRA. We conclude that the earlier finding that myristoylated MSRA is cytosolic was artifactual. It is a late endosomal protein.

Discussion

The major finding reported here is that the nonmitochondrial, myristoylated form of mammalian MSRA binds to STARD3 and is thus located on the cytosolic face of late endosomes, although we do not rule out the possibility that some myristoylated MSRA is in the cytoplasm or other subcellular locations. The interaction between STARD3 and MSRA was demonstrated by 4 independent methods: 1) binding of MSRA to STARD3 on a protein array; 2) localization of GFP-tagged MSRA to late endosomes by immunofluorescence in intact cells; 3) coimmunoprecipitation of STARD3 and MSRA from cell lysates; and 4) subcellular fractionation of cell lysates.

MSRA is known to be myristoylated (15). Although other myristoylated proteins are cytosolic, in general they translocate to membranes under specific conditions (46). We previously considered the possibility that oxidative stress would trigger translocation to a membrane, but application of various oxidative stressors failed to alter its distribution (24). We noted that, "the role of myristoylation remains to be elucidated." The experimental data presented in this study establish that a role of myristoylation is to mediate the binding of MSRA to the cytosolic domain of STARD3.

STARD3 has been known for years to bind cholesterol as well as carotenoids and be a late endosomal protein (36, 40, 44). Although implicated in cholesterol and lipid metabolism, its detailed function was unclear until recently, when Alpy and colleagues (37) established that it mediates the transfer of cholesterol from the endoplasmic reticulum to the endosome. Why MSRA is bound to STARD3 is a matter of speculation at this point, although one can reasonably suggest that MSRA plays a role in lipid/cholesterol metabolism.

In apolipoprotein E-deficient mice, feeding a high-fat "Western diet" causes atherosclerosis and hepatic steatosis. Hepatic overexpression of MSRA in those mice reduced the plasma very low density lipoprotein/low density lipoprotein ratio and reduced the hepatic steatosis and aortic atherosclerosis (47). In humans, a G to A polymorphism in *MSRA* is associated with an increased risk of cardiovascular disease (48, 49). In a genome-wide association study, an A to G intron variant was associated with hypertension, a known risk factor for cardiovascular disease (50).

One possibility is that MSRA provides an oxidative defense for other components in the cholesterol-metabolic pathways. Stocker and colleagues (51, 52) have shown that potentially toxic lipid hydroperoxides are reduced by oxidation of methionine in apolipoproteins to methionine sulfoxide, and MSRA can reduce the sulfoxide in apolipoprotein A-I (53). We showed that MSRA can reduce oxidatively modified Met-307 back to methionine. Met-307 is situated near the distal end of the lipid-binding site and likely binds to STARD3's lipid cargo (40). Met-307 in STARD3 may be particularly susceptible to methionine oxidation by lipid hydroperoxides. The anchoring of MSRA would greatly enhance the efficiency of its action on STARD3. Such a mechanism can explain why myristoylated MSRA protected the mouse heart from ischemia-reperfusion injury, whereas nonmyristoylated, cytosolic MSRA did not (15).

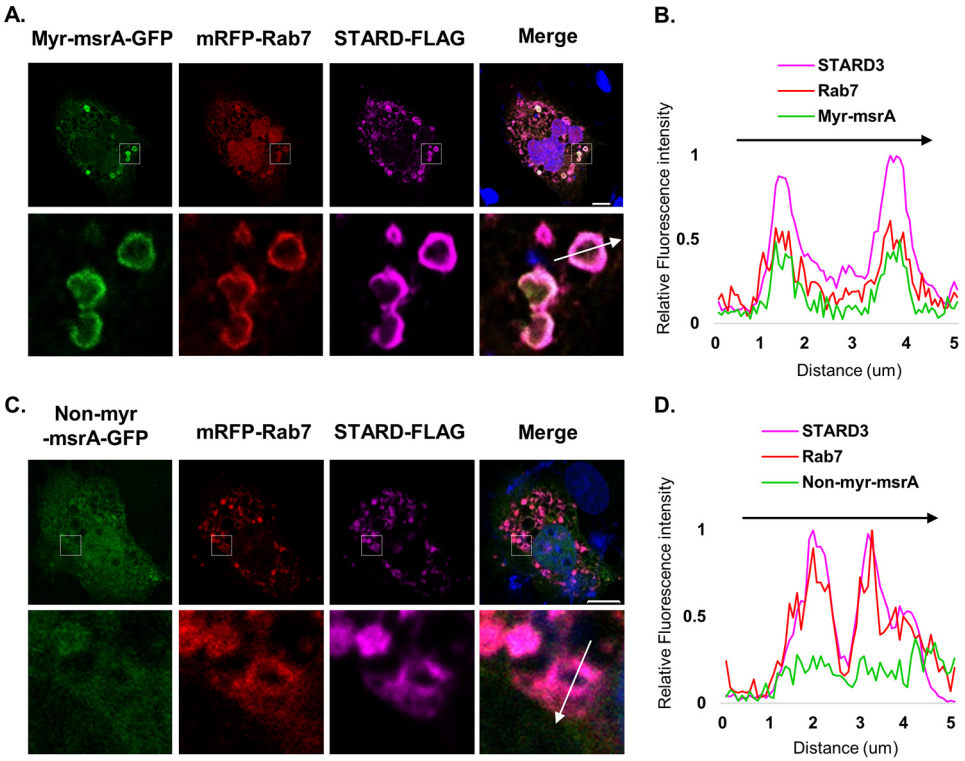

Figure 5. Myristoylated MSRA is anchored to the membrane of late endosomes. *A* and *C,* COS7 cells were transiently transfected with three constructs, *Stard3-FLAG*, *mRFP-Rab7*, a late endosomal protein, and either (*A*) myristoylated *MsrA*-gfp or (*C*) nonmyristoylated *MsrA-gfp*. After 8 h, cells were treated with 20 mM NH_4Cl for 16 h to alkalinize and enlarge late endosomes and lysosomes. The images within the *white box* of the *upper panels* are magnified in the *lower panels*. *Scale bar*, 10 μm. *B* and *D,* the *merged images* were scanned along the *white arrow* for relative fluorescence intensity with ZEN 2 software. The *black arrows* indicate the direction of scanning.

Experimental procedures

Reagents

The monoclonal anti-FLAG antibody was purchased from Origene (TA 50011). The polyclonal rabbit anti-STARD3 antibody for immunoblotting was from MybioSource (MBS 968854) and for immunofluorescence was rabbit anti-MLN64 serum from Abcam (ab3478). Monoclonal mouse anti-STARD3 antibody was obtained from Novusbio (H00010948) and used for immunoprecipitation. Antibody to the early endosome marker EEA1 was a monoclonal mouse anti-EEA1 antibody from BD Biosciences (610457). Antibody to the late endosome/lysosome marker LAMP-1 was a monoclonal mouse anti-LAMP1 antibody obtained from Abcam (ab25630). RAB7 is also a late endosome marker. A mAb against RAB7 that reacts with mouse Rab7 was purchased from Cell Signaling (CS-9367). A polyclonal rabbit anti-HA antibody was purchased from Santa Cruz (sc-805). The antibody against endoplasmic reticulum marker KDEL was a mouse monoclonal from Santa Cruz (sc-58774). A mAb against the mitochondrial marker, mtHSP70, was from Thermo Fisher (MA3-028). The rabbit polyclonal antiserum raised against mouse MSRA was produced in our laboratory (54); it cross-reacts with human MSRA. Specificity was established by comparing the Western blotting of liver from WT and an MSRA knockout mouse (55) (Fig. 6*A*). Protein G-agarose was purchased from Invitrogen (number 15920-010). The siRNA oligomers directed against STARD3 were designed to target to two different regions of human *STARD3*. These oligomers were used: STARD3 siRNA #1, CAAGGGACTTCGTGAATGT (Dharmacon, J-017665-07); STARD3 siRNA #2, GGATGGTGCTGTGGAACAA (Dharmacon, J-017665-08); and nontargeting siRNA control, GGTTTACATGTCGACTAA (Dharmacon, D-001810-01). Restriction enzymes BamHI (R3136), NdeI (R011), and NotI (R3189) were obtained from New England Biolabs, whereas SgfI (R710B) and MluI (R638A) were purchased from Promega.

DNA constructs

Myristoylated and nonmyristoylated human MSRA (residues 23–235) was amplified by PCR and digested with restriction enzymes BamHI and NotI and then inserted into a pCR3.1 vector. Nonmyristoylable MSRA was produced by mutating Gly-24 to Ala by PCR. An inactive form of MSRA was produced by mutating Cys-74 to Ser with the QuikChange site-directed mutagenesis kit (Stratagene). Human MSRA with a C-terminal GFP tag, pCMV6-AC-GFP-MSRA was purchased from Origene (accession number NM_012331, catalogue number RG 208916) and amplified by PCR to generate constructs for myristoylated MSRA and nonmyristoylated MSRA (G24A). A human *STARD3* cDNA clone (NM_006804) in a pCMV6-Myc-FLAG vector was purchased from OriGene (RC206802). To generate truncated forms of START domain, START was amplified by PCR and inserted into a pCMV-Myc-FLAG vector using SgfI and MluI restriction enzymes. The Met-307 and M307R/N311D mutants of the START domain were generated with the QuikChange kit. pDsRed2-Mito was purchased from Clontech (number 6975-1). mRFP-RAB7 was a gift from Ari

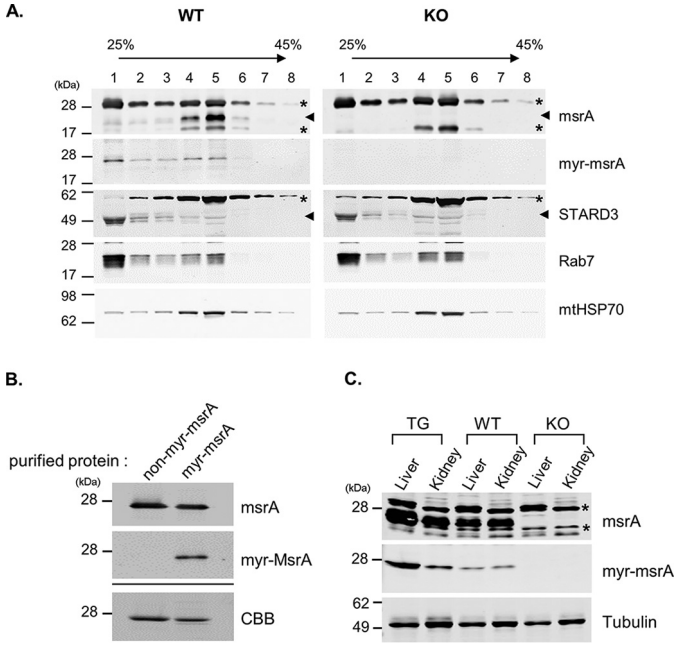

Figure 6. Subcellular fractionation demonstrates that myristoylated MSRA is enriched in the late endosome fraction. *A,* myristoylated MSRA is most prominent in fraction 1 from wildtype (*WT*) mouse liver and is not present in fractions prepared from the MSRA knockout liver (*KO*). Fraction 1 also contains most of the intact late endosomes. Each fraction was evaluated by immunoblot with these marker proteins: RAB7 (late endosome), mtHSP70 (mitochondria), myristoylated MSRA, total MSRA, and STARD3. The *asterisk* (*) indicates a nonspecific band. The molecular size markers of protein are indicated in kDa. The specificity of the mAb for the myristoylated form of MSRA is shown in *panel B*. 100 ng of purified, recombinant human myristoylated or nonmyristoylated MSRA were subjected to SDS-PAGE followed by immunoblotting by either the anti-myristoylated MSRA antibody or the general anti-MSRA antibody. As indicated under "Experimental procedures," the concentration of protein was determined spectrophotometrically. However, to assure that equal amounts of the two proteins were loaded for immunoblotting, we also subjected 1 μg of each protein SDS-PAGE followed by staining with Coomassie Brilliant Blue. *C,* the anti-myristoylated MSRA and general anti-MSRA antibodies are specific for MSRA. This was demonstrated by immunoblotting homogenates of liver and kidney from WT and MSRA knockout mice. The *asterisk* (*) marks nonspecific bands detected by the general anti-MSRA antibody. Tubulin served as a loading control.

Helenius (Addgene plasmid number 14436). Both the WT and G2A *ARF1* plasmids, pXS-*ARF1*-HA, and *Escherichia coli* cells expressing *N*-myristoyltransferase were kindly provided by Dr. Julie G. Donaldson (National Institutes of Health, NHLBI).

Production and purification of recombinant myristoylaed human MSRA(C74S) and nonmyristoylated human MSRA(C74S)

For the myristoylated form, *E. coli* strain BL21(DE3) expressing *N*-myristoyltransferase were transformed with the nonmitochondrial form of human MSRA (residues 23–235, C74S). For the nonmyristoylated form, *E. coli* strain BL21(DE3) cells that did not express *N*-myristoyltransferase were employed. Cells were cultured at 37 °C with 0.5 mM isopropyl 1-thio-β-D-galactopyranoside in 2-liter flasks. After a 4-h induction, cells were collected by centrifugation, resuspended in 50 mM Na_2HPO_4, pH 7.4, with 1× Protease Inhibitor Mixture I (Calbiochem number 539131) and 1 mM phenylmethanesulfonyl chloride (PMSF), and disrupted by French press. The MSRA was purified by anion exchange chromatography (TosoHass DEAE-5PW) followed by hydrophobic interaction chromatography (TosoHass Phenyl-5PW). The expected mass of the purified proteins was confirmed by HPLC-MS (15). They were 23,690 Da for myristoylated human MSRA and 23,480 Da for nonmyristoylated human MSRA.

Production and purification of recombinant human His-STARD3(216–445)

The cytosolic form of STARD3(216–445) with an N-terminal His tag and tobacco etch virus protease-cleavage site was amplified by PCR and digested with restriction enzymes NdeI and BamHI and then inserted into a pET17b vector. BL21 cells were transformed with this His-*Stard3*(216–445) construct, grown at 37 °C in 2-liter flasks, and induced with 0.5 mM isopropyl 1-thio-β-D-galactopyranoside. After a 4-h induction, cells were collected and lysed (50 mM Tris-Cl, pH 8.0, 5 mM imidazole, 100 mM NaCl, 0.1 mM EDTA, 1 mM PMSF with 1× protease inhibitor mixture I).

Lysates were incubated at 4 °C overnight with nickel-nitrilotriacetic acid-agarose beads (Invitrogen, R901-01), after which the beads were washed three times (50 mM Tris-Cl, pH 8.0, 20 mM imidazole, 300 mM NaCl, 0.1 mM EDTA, 1 mM PMSF). Protein was eluted with 50 mM Tris-Cl, pH 8.0, 300 mM imidazole, 50 mM NaCl, 0.1 mM EDTA, and 1 mM PMSF, then dialyzed against 50 mM Tris-Cl, pH 8.0, 150 mM NaCl, and 10 mM DTT. The mass of the purified protein was determined by HPLC-MS (15). The observed mass was 27,773 Da, matching that calculated from the sequence of His-STARD(216–444) (27,773.4 Da). The His tag with tobacco etch virus protease-cleavage site places this sequence to the N terminus: MHHHHHHENLYFQ.

Rabbit mAb specific for myristoylated MSRA

Epitomics (now Abcam) created rabbit hybridomas by immunization against recombinant mouse myristoylated MSRA. The myristoylated and nonmyristoylated mouse MSRA were used to select for a hybridoma with high specificity for the myristoylated form, assayed by Western blotting. Among 53 clones tested, only one was specific for the myristoylated form. The titer of IgG in the supernatant of this clone was very low, leading us to concentrate and purify the IgG. Culture medium from a 1-liter culture (150 mm dishes) was clarified by centrifugation. The supernatant was concentrated to 100 ml and then precipitated with 50% ammonium sulfate. The precipitate was purified by one of two methods. In one, it was dissolved in and dialyzed against 10 mM Tris-HCl, pH 7.5, and purified by protein G-agarose chromatography. In the second, it was dissolved in and dialyzed against 50 mM sodium phosphate, 100 mM NaCl, pH 7.2, and purified by gel filtration chromatography. The purified anti-myristoylated MSRA was stored in aliquots at −80 °C until use. The specificity of the antibody is documented in Fig. 6*B*.

Protein microarray

Myristoylated human MSRA C74S was biotinylated with maleimide-PEG_2-Biotin (Invitrogen, number 21901), and the expected increase in mass of 525.6 Da was confirmed by HPLC-MS. Biotinylated myristoylated MSRA C74S was made 10 μM in washing buffer I (PBS (PBS, KD Medical, 15 mM NaCl, 10 mM

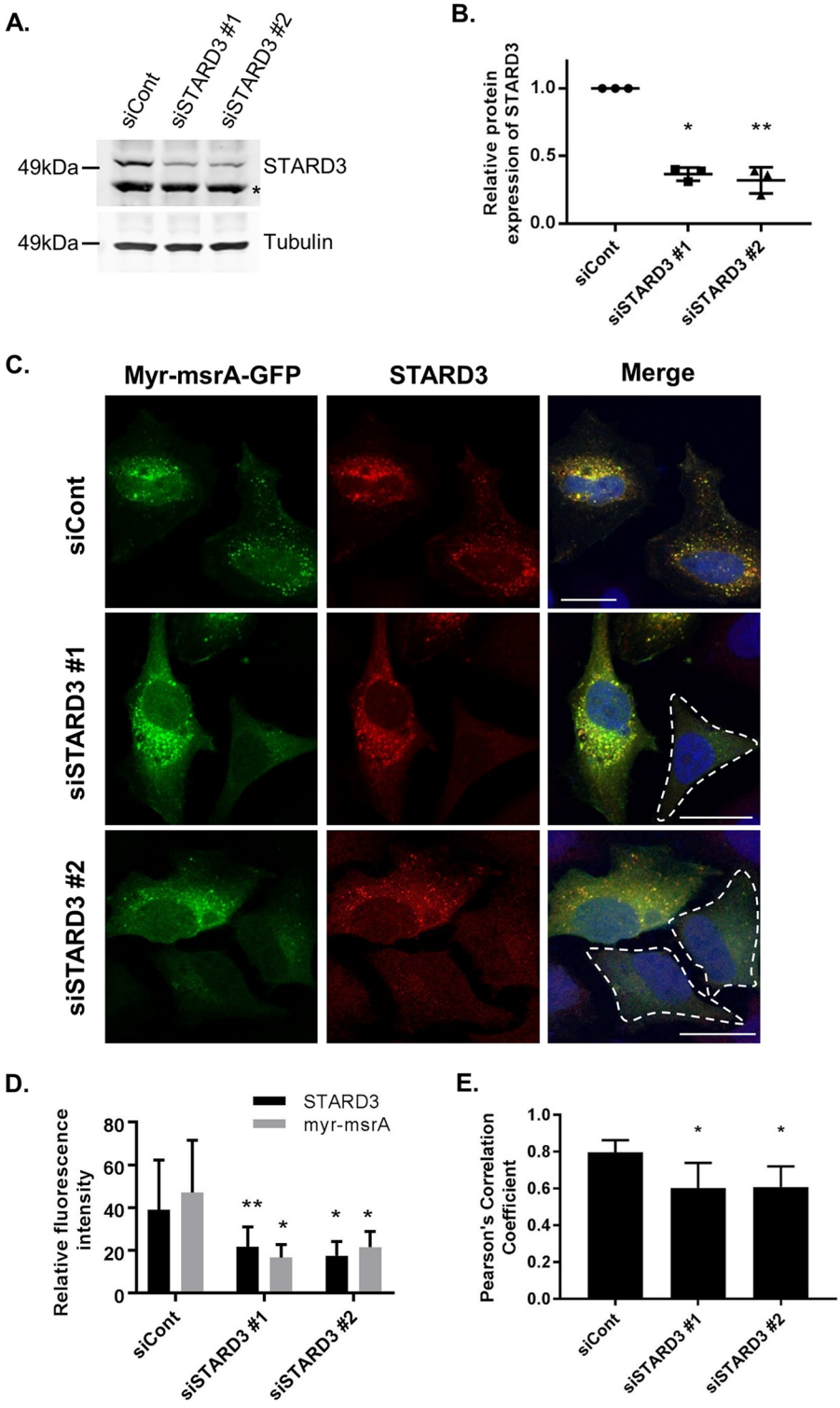

Figure 7. Knocking down STARD3 decreases MSRA on late endosomes. *A,* HeLa cells were transfected for 48 h with nontargeting siRNA (*siCont*) or 2 different *Stard3* targeting oligomers (*siSTARD3 #1* and *siSTARD3 #2*). STARD3 was quantitated by immunoblotting with anti-STARD3, with tubulin serving as a loading control. The *asterisk* (*) marks a nonspecific band. *B,* quantitation of 3 replicates of the experiment shown in *panel A*, run on separate days. The fluorescence intensity of the STARD3 with control siRNA was set to 1.0. The mean ± S.D. are shown as *lines*. Compared with the control using the paired two-tailed *t* test, *, $p < 0.0001$ and **, $p < 0.0003$. *C,* 30 h after transfection with siRNA, HeLa cells were transfected with myristoylated *MsrA-gfp*. 18 h later they were stained with anti-STARD3 antibody. *Scale bar*, 20 μm. The *dashed lines outline* STARD3-depleted cells. 40 such depleted cells were measured for each siRNA and the results shown in *panel D*. *D,* relative fluorescence intensity of myristoylated MSRA and STARD3 was determined using ZEN 2 software (Carl Zeiss) from control and STARD3-depleted cells. 40 cells were analyzed for each sample in 3 independent experiments performed on separate days. The mean ± S.D. are shown as *lines*. Compared with the control using the paired two-tailed *t* test; *, $p < 0.0001$ and **, $p < 0.0002$. *E,* colocalization of myristoylated MSRA and STARD3. 40 cells were analyzed for each sample in 3 independent experiments performed on separate days, and the Pearson's correlation coefficient determined with ImageJ software. The mean ± S.D. are shown as *lines*. Compared with the control siRNA using the paired two-tailed *t* test, *, $p < 0.0001$.

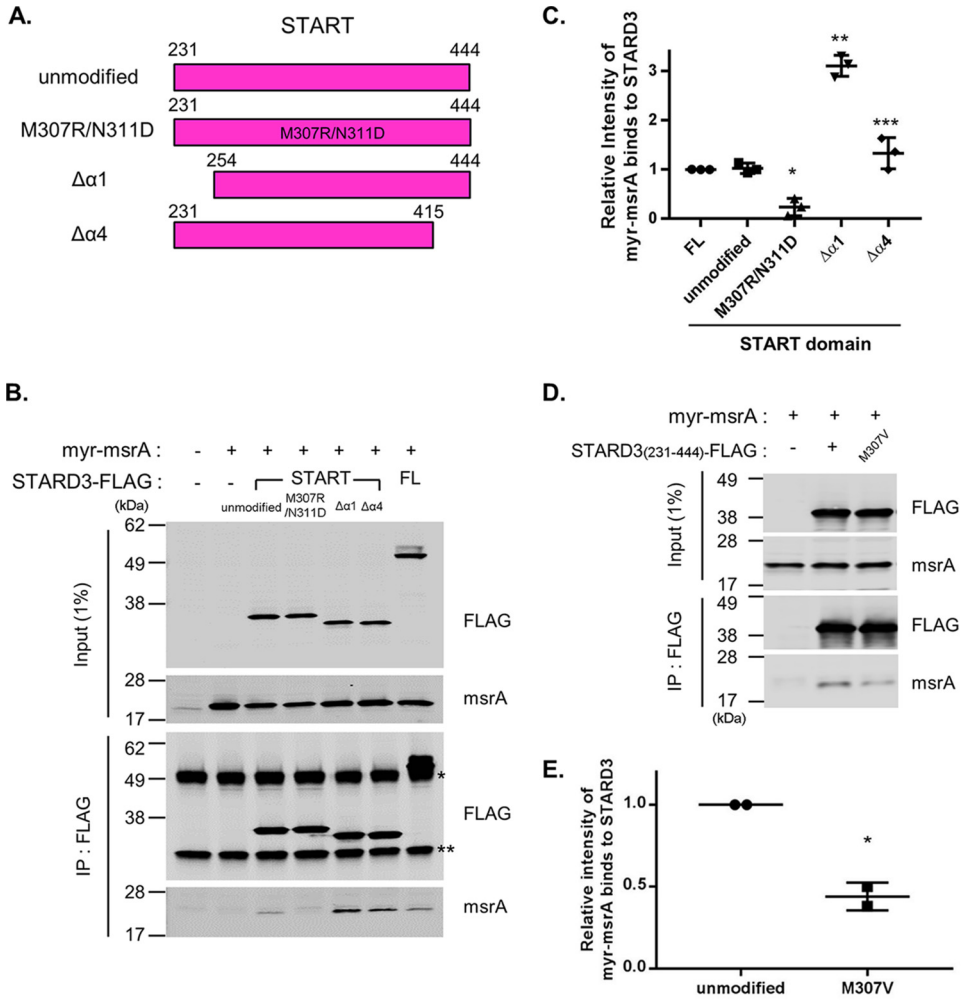

Figure 8. The effect of deletions and mutations on the binding of MSRA to STARD3. The rationale for each construct is given in the text. *A,* diagram of constructs. *B,* HEK293 cells co-expressing myristoylated MSRA and one of the STARD3 shown in *panel A* were immunoprecipitated with anti-FLAG antibody and then probed with anti-MSRA and anti-FLAG antibodies. The *single* and *double asterisks* mark the heavy and light chains of IgG. *C,* quantitation of 3 replicates of the experiment shown in *panel A*, run on separate days. The fluorescence intensity of the full-length STARD3 (*FL*, STARD3(1–444)) was set to 1.0. The mean ± S.D. are shown as *lines*. Compared with the unmodified START domain using the paired two-tailed *t* test: *, $p = 0.003$; **, $p < 0.0001$; ***, $p = 0.18$ *versus* unmodified START domain. *D,* HEK293 cells co-expressing myristoylated MSRA and either unmodified START domain or M307V were immunoprecipitated with anti-FLAG. The protein amounts were measured with anti-FLAG and anti-MSRA. *E,* quantitation of 2 replicates of the experiment shown in *panel D*, run on separate days. The fluorescence intensity of the unmodified protein was set to 1.0. The mean ± S.D. are shown as *lines*. The M307V mutant was compared with the unmodified protein with the two-tailed *t* test, *, $p = 0.01$.

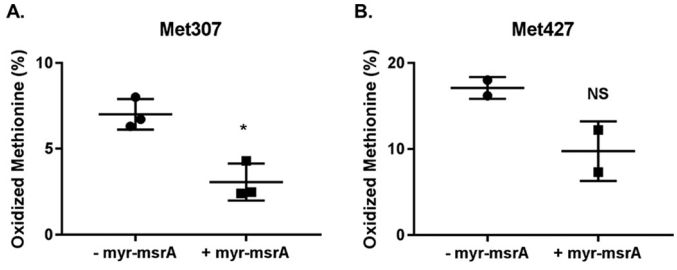

Figure 9. Methionine sulfoxide 307 in oxidatively modified STARD3 is reduced by MSRA. The panels plot the percentage of methionine sulfoxide before and after myristoylated msrA treatment. *A,* Met-307. Three preparations were made and analyzed on separate days. The mean ± S.D. are shown as *lines*. Methionine sulfoxide was reduced in the myristoylated MSRA incubated STARD3 compared with the control using the paired two-tailed *t* test; *, $p = 0.008$. *B,* Met-427. Two preparations were made and analyzed on separate days. The mean ± S.D. are shown as *lines*. *NS*, not significantly different with a paired two-tailed *t* test, $p = 0.11$.

KH_2PO_4, and 56 mM Na_2HPO_4)) with 5% glycerol, 0.05% Triton X-100, 1% BSA, 5 mM $MgCl_2$, and 0.5 mM dithiothreitol (DTT) and incubated with streptavidin-conjugated Alexa 647 (Invitrogen, number S32357) in the dark at room temperature for 1 h. Protein arrays (ProtoArray® Human Protein Microarray version 5.0, Invitrogen) were incubated with blocking buffer (PBS with 0.1% Tween 20 and 1% BSA) for 1 h at 4 °C and then incubated with the biotin-strepavidin complex for 2 h at 4 °C. Arrays were then washed 3 times with washing buffer II (PBS with 0.05% Triton X-100, 1% BSA, 5 mM $MgCl_2$, and 0.5 mM DTT). Arrays were scanned with a GenePix 4200AL and analyzed with Invitrogen Prospector software using the ORF browser database.

Cell culture and immunoprecipitation assays

Mammalian cells were cultured in Dulbecco's modified Eagle's medium (Invitrogen 11965092) including 10% fetal calf serum and 1% penicillin and streptomycin at 37 °C in a humidified atmosphere of 5% CO_2 and 95% air. Cells were transfected using calcium phosphate (Invitrogen, number K278001) for HEK293 cells and Lipofectamine 3000 (Invitrogen, number L3000008) for COS7 and HeLa cells. To deplete STARD3,

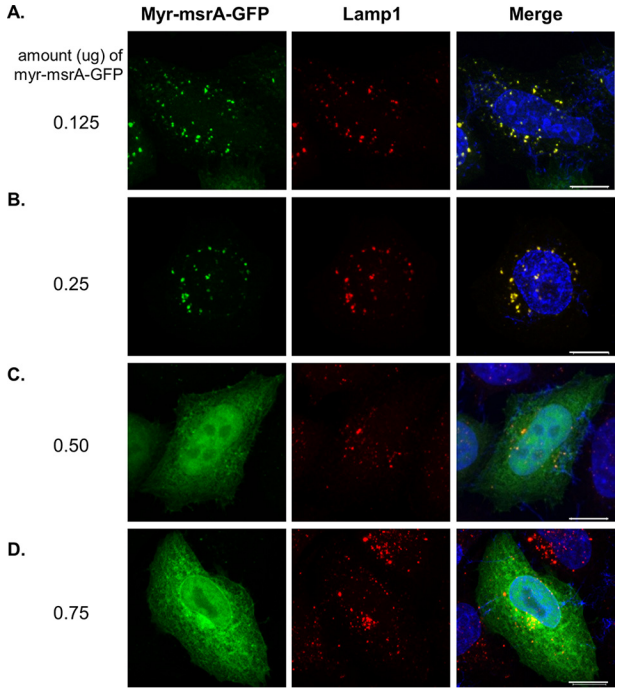

Figure 10. Transfection with higher amounts of DNA causes cytosolic localization of myristoylated MSRA. *A–D,* COS7 cells were transfected with the indicated amount of myristoylated *MsrA-gfp*. After 24 h, cells were stained for the late endosomal marker, LAMP1. *Scale bars*, 10 μm.

COS7 and HeLa cells were transfected with siRNA against STARD3 and nontargeting control for 48 h using Lipofectamine RNAi Max (Invitrogen, number 13778150). For immunoprecipitation assays, HEK293 cells were cotransfected with pCR3.1 human *MsrA* and pCMV *Stard3-FLAG* on 100-mm plates for 24 h and then lysed with 25 mM Tris-HCl, pH 7.4, 150 mM NaCl, 1 mM EDTA, 1% Nonidet P-40, 5% glycerol,1 mM PMSF, and 1× protease inhibitor. Lysates were cleared by centrifugation for 20 min at 20,800 × *g* at 4 °C and then incubated with 3 μg of mouse anti-FLAG antibody (Origene TA50011) for 4 h at 4 °C. Protein-antibody complexes were precipitated with protein G beads for 2 h at 4 °C. Immunoprecipitated proteins were separated by electrophoresis on 10–20% Tris glycine gels (Invitrogen, number XP10205) and transferred to a nitrocellulose membrane (Bio-Rad, number 1704158). Membranes were probed with the indicated antibodies and quantitatively detected by an Odyssey IR scanner (Li-Cor Biosciences).

Subcellular fractionation

To prepare a fraction enriched in late endosomes, subcellular fractionation was performed using a modification of a published procedure (56). 100 mg of liver from WT or MSRA knockout mice was washed with cold PBS. Tissues were gently minced and homogenized on ice with 1 ml of homogenization buffer (250 mM sucrose, 1 mM EDTA, 1 mM PMSF) using a Dounce homogenizer (Wheaton 357542, loose-fitting). After centrifugation at 1,000 × *g* for 10 min, the supernatant was transferred to a new tube and made 25% in sucrose with OptiPrep gradient media (Cosmo Bio USA) in a total volume of 1.5 ml. 2 ml of 45% Opti-Prep was placed in an ultracentrifuge tube for an SW41Ti rotor (Beckman Coulter, 14 × 89 mm). Then 4 ml of 35% OptiPrep was layered on, followed by 3 ml of 25% Opti-Prep. Then the 1.5-ml sample was layered on the top. The tubes were centrifuged for 1 h at 100,000 × *g* after which 1-ml fractions were collected and placed in microcentrifuge tubes. These were centrifuged at 18,000 × *g* for 30 min. The pellet of each fraction was resuspended with 2× sample loading buffer. Following electrophoresis and blotting, the membranes were probed with various antibodies. With this method, late endosomes will be enriched in fractions 1 and 2 (56).

Oxidative modification of STARD3

To generate a low fractional oxidation of the methionine residues in STARD3, 4 μM His-STARD3(216–244) was incubated with 500 μM sodium hypochlorite (Sigma, number 239305) in 20 mM Tris, pH 7.4, with 150 mM sodium chloride for 5 min at 25 °C. Residual hypochlorite was scavenged by the addition of 10 mM DTT after the 5-min incubation. The sample was then divided, with half receiving no additional treatment, whereas the other half was incubated with 4 μM myristoylated MSRA for 30 min at 37 °C. Incubation longer than 30 min did not increase reduction of the STARD3.

Alkylation and tryptic digestion was performed as described (57). HPLC-MS was performed on an Agilent 1200 series HPLC system equipped with an autosampler set to 4 °C and a column compartment set to 30 °C. Separations were performed on a Zorbax 300Å StableBond C18 MicroBore column (1.0 × 50 mm, 3.5 μm particle size, Agilent catalogue number 865630-902). The initial solvent was water, 0.05% TFA and elution was by a gradient with acetonitrile, 0.05% TFA developed at 1%/min with a flow rate of 20 μl/min. The effluent from the column was mixed in a tee with 20 μl/min just prior to the electrospray needle to displace the bound TFA and generate internal standards for the mass spectra (43, 58). Electrospray MS was performed on an Agilent model 6520 accurate mass quadropole-TOF instrument. The effluent-positive electrospray ionization spectra were obtained in the mass range of 100–2500 m/z. The drying gas temperature was 350 °C with a flow rate of 10 liters/min and a nebulizer pressure of 2 bar. The voltages were capillary 3500 V, fragmentor 235 V, skimmer 65 V, and octopole 1 750 V. MS/MS fragmentation used a collision energy of 30 with a data collection range of 20–2000 m/z.

Mass spectra were analyzed using Agilent software, MassHunter version B.05. Extracted ion chromatograms were generated for the methionine and methionine sulfoxide tryptic peptides containing the 2 methionine residues in STARD3, Met-307 and Met-427. We confirmed that the selected peaks were the desired peptides by MS-MS sequencing. The areas of the peaks in the extraction ion chromatogram were used to calculate the percentage of each peptide that was oxidized. The m/z values used to extract chromatograms were 790.4 and 806.4 for reduced and oxidized Met-327 (Z = 1), and 765.6 and 771.0 for reduced and oxidized Met-427 (Z = 3).

Immunofluorescence and confocal microscopy

Cells were seeded on poly-L-lysine-coated coverslips in a 24-well plate and then transfected with various constructs. Cells were fixed with 4% (w/v) paraformaldehyde for 10 min at room temperature and permeabilized with blocking buffer

(PBS, pH 7.4 containing 10% normal goat serum and 0.1% Triton X-100) for 30 min at room temperature. After washing with PBS three times, cells were incubated for 2 h at room temperature or overnight at 4 °C with the following primary antibodies: anti-MSRA (1:100), anti-EEA1 (1:100), anti-LAMP1 (1:50), anti-STARD3 (1:100), or anti-FLAG (1:1000). After washing with PBS, the cells were incubated for 1 h at room temperature with secondary antibodies conjugated to Alexa Fluor 488 (1:500), Alexa Fluor 594 (1:500), or Alexa Fluor 647 (1:500). After washing with PBS, cells were mounted with ProLong Gold Antifade mounting solution containing DAPI for nuclear staining (Invitrogen). Slides were visualized with a confocal laser scanning microscope, LSM780 or LSM880 Airyscan (Zeiss) and analyzed with ZEN 2 software (Carl Zeiss). The colocalization of myristoylated MSRA and STARD3 was performed on the raw pixel data by Pearson's correlation coefficient using ImageJ software.

Author contributions—J. M. L. and R. L. L. formal analysis; J. M. L. validation; J. M. L., J. C. L., G. K., and R. L. L. investigation; J. M. L. visualization; J. M. L. and G. K. methodology; J. M. L. and R. L. L. writing-original draft; J. C. L. and R. L. L. conceptualization; G. K. and R. L. L. supervision; R. L. L. funding acquisition; R. L. L. writing-review and editing.

Acknowledgments—We are grateful to Drs. Matthias Machner and Nicole Ellis for introducing us to protein arrays. We thank Dr. Julie Donaldson for helpful guidance and for providing the expression vectors for ARF1. We sincerely thank the anonymous reviewers whose suggestions substantially improved this paper. Confocal microscopy was performed on instruments in the Light Microscopy Core of the National Heart, Lung, and Blood Institute.

References

1. Levine, R. L., Mosoni, L., Berlett, B. S., and Stadtman, E. R. (1996) Methionine residues as endogenous antioxidants in proteins. *Proc. Natl. Acad. Sci. U.S.A.* **93,** 15036–15040 CrossRef Medline
2. Bender, A., Hajieva, P., and Moosmann, B. (2008) Adaptive antioxidant methionine accumulation in respiratory chain complexes explains the use of a deviant genetic code in mitochondria. *Proc. Natl. Acad. Sci. U.S.A.* **105,** 16496–16501 CrossRef Medline
3. Valley, C. C., Cembran, A., Perlmutter, J. D., Lewis, A. K., Labello, N. P., Gao, J., and Sachs, J. N. (2012) The methionine-aromatic motif plays a unique role in stabilizing protein structure. *J. Biol. Chem.* **287,** 34979–34991 CrossRef Medline
4. Lee, B. C., Péterfi, Z., Hoffmann, F. W., Moore, R. E., Kaya, A., Avanesov, A., Tarrago, L., Zhou, Y., Weerapana, E., Fomenko, D. E., Hoffmann, P. R., and Gladyshev, V. N. (2013) MsrB1 and MICALs regulate actin assembly and macrophage function via reversible stereoselective methionine oxidation. *Mol. Cell* **51,** 397–404 CrossRef Medline
5. Hung, R. J., Spaeth, C. S., Yesilyurt, H. G., and Terman, J. R. (2013) SelR reverses Mical-mediated oxidation of actin to regulate F-actin dynamics. *Nat. Cell. Biol.* **15,** 1445–1454 CrossRef Medline
6. Hung, R.-J., Pak, C. W., and Terman, J. R. (2011) Direct redox regulation of F-actin assembly and disassembly by mical. *Science* **334,** 1710–1713 CrossRef Medline
7. Netzer, N., Goodenbour, J. M., David, A., Dittmar, K. A., Jones, R. B., Schneider, J. R., Boone, D., Eves, E. M., Rosner, M. R., Gibbs, J. S., Embry, A., Dolan, B., Das, S., Hickman, H. D., Berglund, P., *et al.* (2009) Innate immune and chemically triggered oxidative stress modifies translational fidelity. *Nature* **462,** 522–526 CrossRef Medline
8. Lee, J. Y., Kim, D. G., Kim, B. G., Yang, W. S., Hong, J., Kang, T., Oh, Y. S., Kim, K. R., Han, B. W., Hwang, B. J., Kang, B. S., Kang, M. S., Kim, M. H., Kwon, N. H., and Kim, S. (2014) Promiscuous methionyl-tRNA synthetase mediates adaptive mistranslation to protect cells against oxidative stress. *J. Cell Sci.* **127,** 4234–4245 CrossRef Medline
9. Lavine, T. F. (1947) The formation, resolution, and optical properties of the diasteriomeric sulfoxides derived from L-methionine. *J. Biol. Chem.* **169,** 477–491 Medline
10. Vogt, W. (1995) Oxidation of methionine residues in proteins: tools, targets, and reversal. *Free Radic. Biol. Med.* **18,** 93–105 CrossRef Medline
11. Toennies, G., and Kolb, J. J. (1939) Methionine studies: IV. a color reaction to methionine. *J. Biol. Chem.* **128,** 399–405
12. Weissbach, H., Resnick, L., and Brot, N. (2005) Methionine sulfoxide reductases: history and cellular role in protecting against oxidative damage. *Biochim. Biophys. Acta* **1703,** 203–212 CrossRef Medline
13. Lee, B. C., Dikiy, A., Kim, H. Y., and Gladyshev, V. N. (2009) Functions and evolution of selenoprotein methionine sulfoxide reductases. *Biochim. Biophys. Acta* **1790,** 1471–1477 CrossRef Medline
14. Boschi-Muller, S., Gand, A., and Branlant, G. (2008) The methionine sulfoxide reductases: catalysis and substrate specificities. *Arch. Biochem. Biophys.* **474,** 266–273 CrossRef Medline
15. Kim, G., Cole, N. B., Lim, J. C., Zhao, H., and Levine, R. L. (2010) Dual sites of protein initiation control the localization and myristoylation of methionine sulfoxide reductase A. *J. Biol. Chem.* **285,** 18085–18094 CrossRef Medline
16. Kim, H. Y., and Gladyshev, V. N. (2005) Role of structural and functional elements of mouse methionine-S-sulfoxide reductase in its subcellular distribution. *Biochemistry* **44,** 8059–8067 CrossRef Medline
17. Zhao, H., Sun, J., Deschamps, A. M., Kim, G., Liu, C., Murphy, E., and Levine, R. L. (2011) Myristoylated methionine sulfoxide reductase A protects the heart from ischemia-reperfusion injury. *Am. J. Physiol. Heart Circ. Physiol.* **301,** H1513–H1518 CrossRef Medline
18. Lim, J. C., Gruschus, J. M., Ghesquière, B., Kim, G., Piszczek, G., Tjandra, N., and Levine, R. L. (2012) Characterization and solution structure of mouse myristoylated methionine sulfoxide reductase A. *J. Biol. Chem.* **287,** 25589–25595 CrossRef Medline
19. Lim, J. C., Kim, G., and Levine, R. L. (2013) Stereospecific oxidation of calmodulin by methionine sulfoxide reductase A. *Free Radic. Biol. Med.* **61,** 257–264 CrossRef Medline
20. Ubbink, M. (2009) The courtship of proteins: understanding the encounter complex. *FEBS Lett.* **583,** 1060–1066 CrossRef Medline
21. Moskovitz, J., Bar-Noy, S., Williams, W. M., Requena, J., Berlett, B. S., and Stadtman, E. R. (2001) Methionine sulfoxide reductase (MsrA) is a regulator of antioxidant defense and lifespan in mammals. *Proc. Natl. Acad. Sci. U.S.A.* **98,** 12920–12925 CrossRef Medline
22. Moskovitz, J., Berlett, B. S., Poston, J. M., and Stadtman, E. R. (1997) The yeast peptide-methionine sulfoxide reductase functions as an antioxidant *in vivo*. *Proc. Natl. Acad. Sci. U.S.A.* **94,** 9585–9589 CrossRef Medline
23. Moskovitz, J., Rahman, M. A., Strassman, J., Yancey, S. O., Kushner, S. R., Brot, N., and Weissbach, H. (1995) *Escherichia coli* peptide methionine sulfoxide reductase gene: regulation of expression and role in protecting against oxidative damage. *J. Bacteriol.* **177,** 502–507 CrossRef Medline
24. Douglas, T., Daniel, D. S., Parida, B. K., Jagannath, C., and Dhandayuthapani, S. (2004) Methionine sulfoxide reductase A (MsrA) deficiency affects the survival of *Mycobacterium smegmatis* within macrophages. *J. Bacteriol.* **186,** 3590–3598 CrossRef Medline
25. St John, G., Brot, N., Ruan, J., Erdjument-Bromage, H., Tempst, P., Weissbach, H., and Nathan, C. (2001) Peptide methionine sulfoxide reductase from *Escherichia coli* and *Mycobacterium tuberculosis* protects bacteria against oxidative damage from reactive nitrogen intermediates. *Proc. Natl. Acad. Sci. U.S.A.* **98,** 9901–9906 CrossRef Medline
26. Mahawar, M., Tran, V., Sharp, J. S., and Maier, R. J. (2011) Synergistic roles of *Helicobacter pylori* methionine sulfoxide reductase and GroEL in repairing oxidant-damaged catalase. *J. Biol. Chem.* **286,** 19159–19169 CrossRef Medline
27. Ruan, H., Tang, X. D., Chen, M. L., Joiner, M. L., Sun, G., Brot, N., Weissbach, H., Heinemann, S. H., Iverson, L., Wu, C. F., Hoshi, T., Chen, M. L., Joiner, M. A., and Heinemann, S. H. (2002) High-quality life extension by the enzyme peptide methionine sulfoxide reductase. *Proc. Natl. Acad. Sci. U.S.A.* **99,** 2748–2753 CrossRef Medline

28. Moskovitz, J., Flescher, E., Berlett, B. S., Azare, J., Poston, J. M., and Stadtman, E. R. (1998) Overexpression of peptide-methionine sulfoxide reductase in *Saccharomyces cerevisiae* and human T cells provides them with high resistance to oxidative stress. *Proc. Natl. Acad. Sci. U.S.A.* **95,** 14071–14075 CrossRef Medline
29. Romero, H. M., Berlett, B. S., Jensen, P. J., Pell, E. J., and Tien, M. (2004) Investigations into the role of the plastidial peptide methionine sulfoxide reductase in response to oxidative stress in Arabidopsis. *Plant Physiol.* **136,** 3784–3794 CrossRef Medline
30. Yermolaieva, O., Xu, R., Schinstock, C., Brot, N., Weissbach, H., Heinemann, S. H., and Hoshi, T. (2004) Methionine sulfoxide reductase A protects neuronal cells against brief hypoxia/reoxygenation. *Proc. Natl. Acad. Sci. U.S.A.* **101,** 1159–1164 CrossRef Medline
31. Benoit, S. L., and Maier, R. J. (2016) *Helicobacter* catalase devoid of catalytic activity protects the bacterium against oxidative stress. *J. Biol. Chem.* **291,** 23366–23373 CrossRef Medline
32. Wang, X., and Pan, T. (2016) Stress response and adaptation mediated by amino acid misincorporation during protein synthesis. *Adv. Nutr.* **7,** 773s–779s CrossRef Medline
33. Lim, J. C., You, Z., Kim, G., and Levine, R. L. (2011) Methionine sulfoxide reductase A is a stereospecific methionine oxidase. *Proc. Natl. Acad. Sci. U.S.A.* **108,** 10472–10477 CrossRef Medline
34. Ghesquiere, B., Jonckheere, V., Colaert, N., Van Durme, J., Timmerman, E., Goethals, M., Schymkowitz, J., Rousseau, F., Vandekerckhove, J., and Gevaert, K. (2011) Redox proteomics of protein-bound methionine oxidation. *Mol. Cell. Proteomics* **10,** CrossRef
35. Suchanek, M., Radzikowska, A., and Thiele, C. (2005) Photo-leucine and photo-methionine allow identification of protein-protein interactions in living cells. *Nat. Meth.* **2,** 261–268 CrossRef
36. Alpy, F., Stoeckel, M. E., Dierich, A., Escola, J. M., Wendling, C., Chenard, M. P., Vanier, M. T., Gruenberg, J., Tomasetto, C., and Rio, M. C. (2001) The steroidogenic acute regulatory protein homolog MLN64, a late endosomal cholesterol-binding protein. *J. Biol. Chem.* **276,** 4261–4269 CrossRef Medline
37. Wilhelm, L. P., Wendling, C., Védie, B., Kobayashi, T., Chenard, M. P., Tomasetto, C., Drin, G., and Alpy, F. (2017) STARD3 mediates endoplasmic reticulum-to-endosome cholesterol transport at membrane contact sites. *EMBO J.* **36,** 1412–1433 CrossRef Medline
38. Alpy, F., and Tomasetto, C. (2014) START ships lipids across interorganelle space. *Biochimie (Paris)* **96,** 85–95 CrossRef
39. Thermo Fisher Scientific. (2015) ProtoArray® Applications Guide, Thermo Fisher Scientific, Waltham, MA
40. Tsujishita, Y., and Hurley, J. H. (2000) Structure and lipid transport mechanism of a StAR-related domain. *Nat. Struct. Mol. Biol.* **7,** 408–414 CrossRef
41. Donaldson, J. G., Honda, A., and Weigert, R. (2005) Multiple activities for Arf1 at the Golgi complex. *Biochim. Biophys. Acta* **1744,** 364–373 CrossRef Medline
42. Alpy, F., Latchumanan, V. K., Kedinger, V., Janoshazi, A., Thiele, C., Wendling, C., Rio, M. C., and Tomasetto, C. (2005) Functional characterization of the MENTAL domain. *J. Biol. Chem.* **280,** 17945–17952 CrossRef Medline
43. Levine, R. L. (2006) Fixation of nitrogen in an electrospray mass spectrometer. *Rapid. Commun. Mass Spectrom.* **20,** 1828–1830 CrossRef Medline
44. Horvath, M. P., George, E. W., Tran, Q. T., Baumgardner, K., Zharov, G., Lee, S., Sharifzadeh, H., Shihab, S., Mattinson, T., Li, B., and Bernstein, P. S. (2016) Structure of the lutein-binding domain of human StARD3 at 1.74-Å resolution and model of a complex with lutein. *Acta Crystallogr. Sect. F Struct. Biol. Commun.* **72,** 609–618 CrossRef
45. Perricone, N., Nagy, K., Horváth, F., Dajkó, G., Uray, I., and Nagy, I. (1999) α-Lipoic acid (ALA) protects proteins against the hydroxyl free radical-induced alterations: rationale for its geriatric topical application. *Arch. Gerontol. Geriatr.* **29,** 45–56 CrossRef Medline
46. Resh, M. D. (2006) Trafficking and signaling by fatty-acylated and prenylated proteins. *Nat. Chem. Biol.* **2,** 584–590 CrossRef
47. Xu, Y. Y., Du, F., Meng, B., Xie, G. H., Cao, J., Fan, D., and Yu, H. (2015) Hepatic overexpression of methionine sulfoxide reductase A reduces atherosclerosis in apolipoprotein E-deficient mice. *J. Lipid Res.* **56,** 1891–1900 CrossRef Medline
48. García-Bermúdez, M., López-Mejías, R., González-Juanatey, C., Castañeda, S., Miranda-Filloy, J. A., Blanco, R., Fernández-Gutiérrez, B., Balsa, A., González-Álvaro I, Gómez-Vaquero, C., Llorca, J., Martín, J., and González-Gay, M. A. (2012) Association of the methionine sulfoxide reductase A rs10903323 gene polymorphism with cardiovascular disease in patients with rheumatoid arthritis. *Scand. J. Rheumatol.* **41,** 350–353 CrossRef Medline
49. Gu, H., Chen, W., Yin, J., Chen, S., Zhang, J., and Gong, J. (2013) Methionine sulfoxide reductase A rs10903323 G/A polymorphism is associated with increased risk of coronary artery disease in a Chinese population. *Clin. Biochem.* **46,** 1668–1672 CrossRef Medline
50. Levy, D., Ehret, G. B., Rice, K., Verwoert, G. C., Launer, L. J., Dehghan, A., Glazer, N. L., Morrison, A. C., Johnson, A. D., Aspelund, T., Aulchenko, Y., Lumley, T., Köttgen, A., Vasan, R. S., Rivadeneira, F., *et al.* (2009) Genome-wide association study of blood pressure and hypertension. *Nat. Genet.* **41,** 677–687 CrossRef Medline
51. Garner, B., Witting, P. K., Waldeck, A. R., Christison, J. K., Raftery, M., and Stocker, R. (1998) Oxidation of high density lipoproteins: I. formation of methionine sulfoxide in apolipoproteins AI and AII is an early event that accompanies lipid peroxidation and can be enhanced by α-tocopherol. *J. Biol. Chem.* **273,** 6080–6087 CrossRef Medline
52. Garner, B., Waldeck, A. R., Witting, P. K., Rye, K. A., and Stocker, R. (1998) Oxidation of high density lipoproteins: II. evidence for direct reduction of lipid hydroperoxides by methionine residues of apolipoproteins AI and AII. *J. Biol. Chem.* **273,** 6088–6095 CrossRef Medline
53. Sigalov, A. B., and Stern, L. J. (1998) Enzymatic repair of oxidative damage to human apolipoprotein A-I. *FEBS Lett.* **433,** 196–200 CrossRef Medline
54. Cole, N. B., Daniels, M. P., Levine, R. L., and Kim, G. (2010) Oxidative stress causes reversible changes in mitochondrial permeability and structure. *Exp. Gerontol.* **45,** 596–602 CrossRef Medline
55. Salmon, A. B., Pérez, V. I., Bokov, A., Jernigan, A., Kim, G., Zhao, H., Levine, R. L., and Richardson, A. (2009) Lack of methionine sulfoxide reductase A in mice increases sensitivity to oxidative stress but does not diminish life span. *FASEB J.* **23,** 3601–3608 CrossRef Medline
56. Walker, L. R., Hussein, H. A., and Akula, S. M. (2016) Subcellular fractionation method to study endosomal trafficking of Kaposi's sarcoma-associated herpesvirus. *Cell Biosci.* **6,** 1 Medline
57. Chen, J., Teixeira, P. F., Glaser, E., and Levine, R. L. (2014) Mechanism of oxidative inactivation of human presequence protease by hydrogen peroxide. *Free Radic. Biol. Med.* **77,** 57–63 CrossRef Medline
58. Apffel, A., Fischer, S., Goldberg, G., Goodley, P. C., and Kuhlmann, F. E. (1995) Enhanced sensitivity for peptide mapping with electrospray liquid chromatography-mass spectrometry in the presence of signal suppression due to trifluoroacetic acid-containing mobile phases. *J. Chromatogr. A* **712,** 177–190 CrossRef Medline